Inhomogeneous magnetism in La-doped $CaMnO_3$. I. Mesoscopic phase separation due to lattice-coupled ferromagnetic interactions

C. D. Ling,[1,2,*] E. Granado,[3,4,5] J. J. Neumeier,[6] J. W. Lynn,[3,4] and D. N. Argyriou[2,7]
[1]*Institut Laue-Langevin, BP 156, 38042 Grenoble Cedex 9, France*
[2]*Materials Science Division, Argonne National Laboratory, Argonne, Illinois 60439, USA*
[3]*NIST Center for Neutron Research, National Institute of Standards and Technology, Gaithersburg, Maryland 20899, USA*
[4]*Center for Superconductivity Research, University of Maryland, College Park, Maryland 20742, USA*
[5]*Laboratório Nacional de Luz Síncrotron, Caixa Postal 6192, CEP 13084-971, Campinas, SP, Brazil*
[6]*Department of Physics, Montana State University, Bozeman, Montana 59717, USA*
[7]*Hahn-Meitner-Institut, Glienicker str. 100, Berlin D-14109, Germany*
(Received 14 March 2003; published 23 October 2003)

A detailed investigation of mesoscopic magnetic and crystallographic phase separation in $Ca_{1-x}La_xMnO_3$, $0.00 \leqslant x \leqslant 0.20$, is reported. Neutron powder diffraction and dc-magnetization techniques have been used to isolate the different roles played by electrons doped into the e_g level as a function of their concentration x. The presence of multiple low-temperature magnetic and crystallographic phases within individual polycrystalline samples is argued to be an intrinsic feature of the system that follows from the shifting balance between competing ferromagnetic (FM) and antiferromagnetic (AFM) interactions as a function of temperature. FM double-exchange interactions associated with doped e_g electrons are favored over competing AFM interactions at higher temperatures, and couple more strongly with the lattice *via* orbital polarization. These FM interactions thereby play a privileged role, even at low e_g electron concentrations, by virtue of structural modifications induced above the AFM transition temperatures.

DOI: 10.1103/PhysRevB.68.134439 PACS number(s): 75.25.+z, 61.12.Ld, 75.30.Kz, 75.70.Kw

I. INTRODUCTION

The physical properties of mixed valent perovskite manganites such as $Ca_{1-x}La_xMnO_3$ are dominated by the strong coupling of charge-orbital and spin degrees of freedom. This results in a family of materials that shows pronounced physical property responses to chemical doping, temperature, pressure, and magnetic field. Of these responses, colossal magnetoresistance (CMR)—a dramatic drop in resistivity in an applied magnetic field—at optimal doping $x \sim 0.7$ has attracted the most attention as it raises the possibility of applications such as data storage devices and sensors.

At the ''electron-doped'' end of the phase diagram ($x \sim 0$), the light doping of charges into the well understood G-type antiferromagnetic [G-AFM, Fig. 1(a)] ground state provides an opportunity to test the relevance of physical models of manganites. It was originally argued by de Gennes[1] that a small concentration of doped carriers into the e_g band (which is fully polarized due to the strong Hund's coupling of localized t_{2g} electrons) gives rise to ferromagnetic (FM) double-exchange (DE) interactions, which for lightly doped systems competes with AFM super-exchange (SE) to produce a spin canted G-AFM state.[2] This is consistent with a coexistence of FM and G-AFM components observed by neutron powder diffraction (NPD).[3–7] The application of simple DE across the whole of the phase diagram, however, contradicts experimental evidence by predicting either homogenous canting or the pure FM state at all points, in contrast with the rich phase diagram experimentally observed.[8] In fact, the (ostensibly) spin-canted state only survives to $x \sim 0.1$, beyond which the degeneracy of the ($d_{x^2-y^2}$ and $d_{3z^2-r^2}$) e_g orbitals causes it to be supplanted by C-type AFM [C-AFM, Fig 1(b)].[4,6,8,9] In C-AFM, FM DE becomes long range in one dimension via delocalized $d_{3z^2-r^2}$ orbital chains, into which the doped e_g electrons are stabilized, while AFM SE is maintained perpendicular to these chains. This leads to a cooperative Jahn-Teller (JT) distortion along the FM chain direction, lowering the symmetry from orthorhombic P*nma* to monoclinic $P2_1/m$.

These two papers report a detailed investigation into the nature of, and the relationships among, the rich variety of phases found in the electron-doped regime of $Ca_{1-x}La_xMnO_3$. This is of interest both as a model for spin-lattice coupling in the dilute limit of lattice polarons, and due to reports in many systems $Ca_{1-x}A_xMnO_3$ of large magnetoresistance effects[10–14] and metamagnetic phase transitions.[6,15] Part I concerns principally the relationships among the various crystallographic (orthorhombic and monoclinic) and magnetic (G-AFM, liquid-like FM clusters, FM cluster glass and C-AFM) phases. High-resolution NPD and dc-magnetization techniques are used to address questions of sample homogeneity arising out of the observation of multiple crystallographic and magnetic phases in individual polycrystalline samples,[4,13,16] necessary in order to correctly interpret local phenomenon observed using bulk probes. It is found that the inability to attain a unique thermodynamic ground state is an intrinsic feature of the system resulting from the extremely fine balance between competing states. In Part II,[16] we find using neutron scattering that for light electron-doping $0.0 < x \lesssim 0.1$, the G-AFM matrix contains a well-organized liquid distribution of FM clusters ~ 10 Å in diameter. These clusters can be aligned by an external applied magnetic field to produce a long-range FM moment, as seen at the opposite end of the same phase

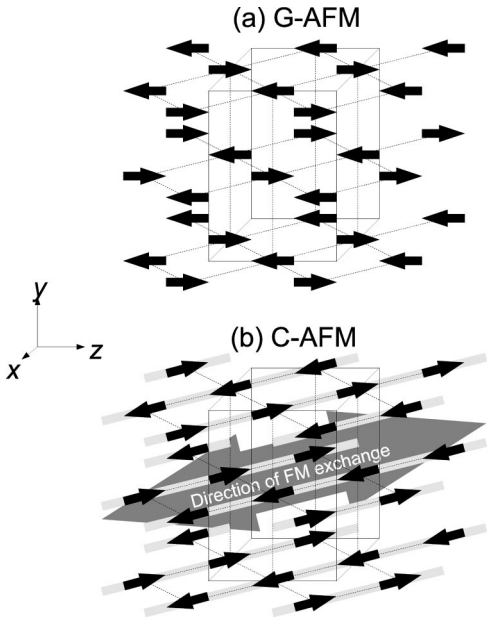

FIG. 1. Schematic representations of the low-T magnetic ground states of $Ca_{1-x}La_xMnO_3$ ($x \lesssim 0.2$). Solid lines show the unit cell and dashed lines show nearest-neighbor Mn-Mn interactions. (a) Ideal G-AFM. (b) C-AFM, in which e_g electrons delocalize into $d_{3z^2-y^2}$ orbital chains along the $(10\bar{1})$ direction, allowing 1D FM DE while maintaining AFM interactions among the chains and causing a symmetry-lowering from orthorhombic P*nma* to monoclinic $P2_1/m$.

diagram.[17–19] The higher density of these clusters at $x=0.09$ leads to a spontaneous ($H=0$) long-range FM moment due to the formation of a FM cluster glass,[20] the orientation of which is coupled to the G-AFM matrix.

II. EXPERIMENTAL DETAILS

Ceramic samples of $Ca_{1-x}La_xMnO_3$ with nominal compositions $0.00 \leqslant x \leqslant 0.20$ were prepared by solid state reaction. Stoichiometric quantities of (99.99% purity or better) $CaCO_3$, La_2O_3, and MnO_2 were weighed (to yield 7 g samples) and mixed in an agate mortar for 15 min followed by reaction for 20 h at 1100 °C. The specimens were reground for 10 min, reacted for 20 h at 1150 °C, reground for 10 min, reacted for 20 h at 1250 °C, reground for 10 min, reacted for 46 h at 1300 °C, reground for 10 min, reacted for 46 h at 1300 °C, reground for 10 min, pressed into pellets, reacted for 17 h at 1300 °C, and cooled at 0.4 °C min^{-1} to 30 °C. Identically prepared samples in the same composition range[25] were iodometrically titrated to measure the average Mn valence, indicating that the oxygen content of all specimens fell within the range 3.00 ± 0.01.

dc-magnetization measurements were conducted using a commercially available superconducting quantum interference device magnetometer. Specimens were cooled to 5 K in zero field, then warmed to the highest measurement temperature in an applied field of $H=2000$ Oe. Magnetization vs H curves were taken at 5 K.

Temperature-dependent time-of-flight (TOF) NPD data were collected on the Special Environment Powder Diffractometer (SEPD) at Argonne National Laboratory's Intense Pulsed Neutron Source (IPNS). Data were analyzed by Rietveld refinement using the program suite FullProf. 1–2-wt. % Marokite ($CaMn_2O_4$) (Refs. 21 and 22) impurities were included in all refinements as both nuclear and (at low temperatures) magnetic phases (details of the low-T AFM structure of Marokite are published elsewhere).[23]

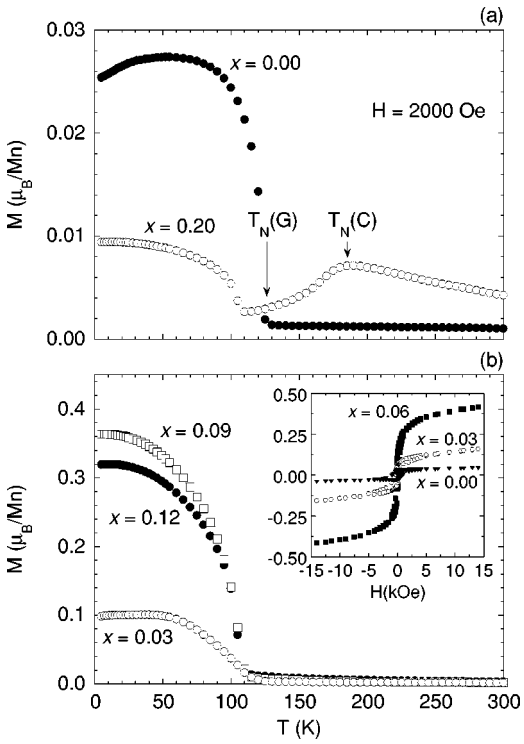

FIG. 2. (a) Magnetization M vs T measured at $H=2000$ Oe for $x=0.00$ and 0.20 samples. T_N(C) and T_N(G) are indicated. (b) A similar plot (note the change in scale) for $x=0.03$, 0.09 and 0.12 samples, with an inset showing M vs H for $x=0.00$, 0.03 and 0.06. For the M vs H loops, lines were drawn through the low and high field regions of the data, and the intersection taken as the saturation moment M_{sat} at 5 K used in Fig. 3.

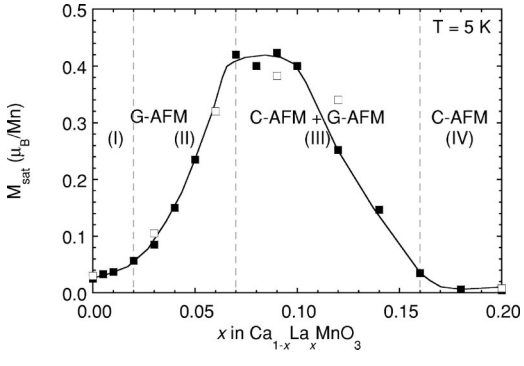

FIG. 3. Magnetic saturation moments M_{sat} determined from M vs H curves at 5 K for the samples used in the present study (open squares) and in the study by Neumeier and Cohn (Ref. 25) (solid squares) as a function of x. Regions (I)–(IV) discussed by Neumeier and Cohn are labeled and defined by dashed lines.

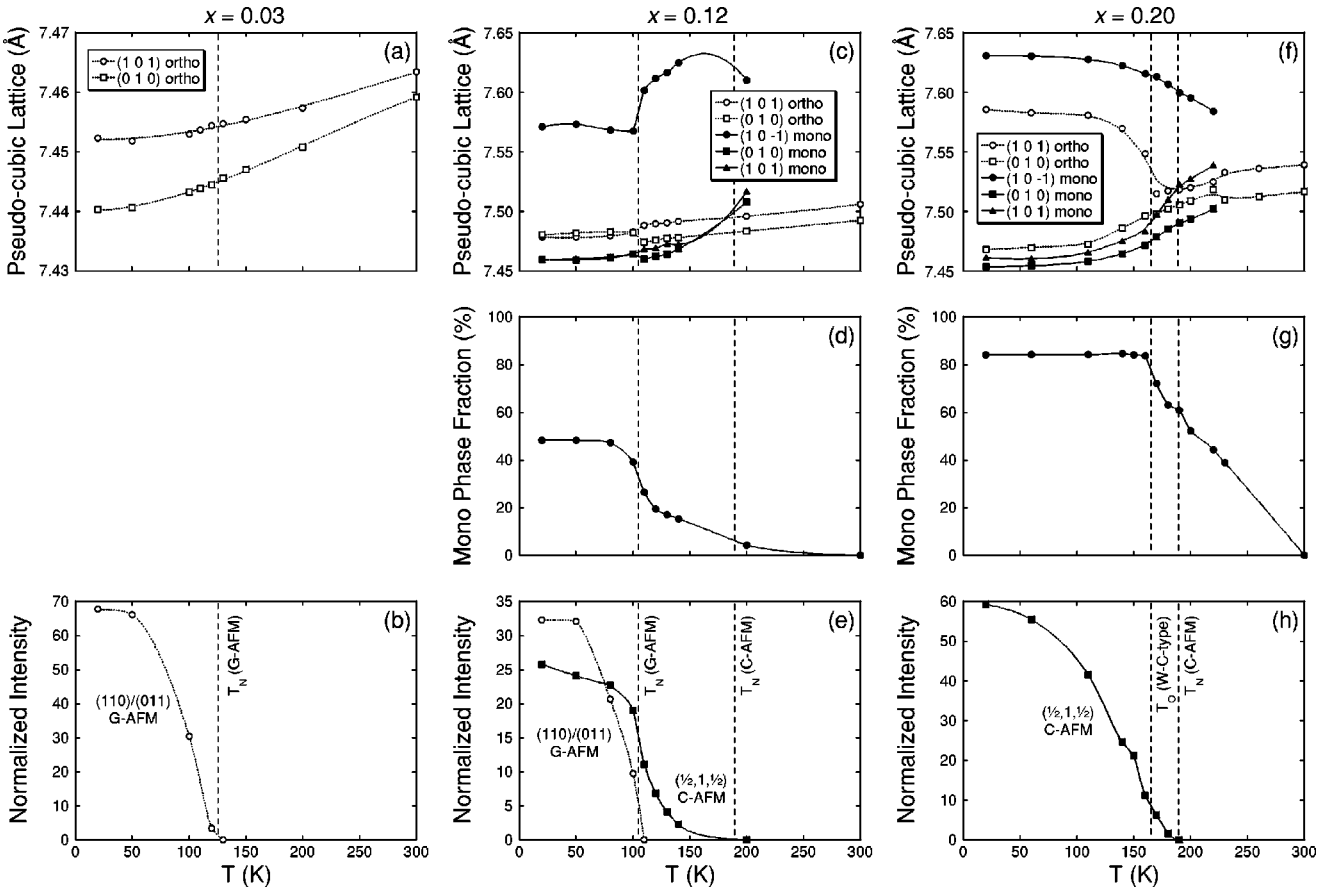

FIG. 4. (a), (c), and (f) T dependence of pseudocubic lattice parameters along (101), $(10\bar{1})$, and (010) for (a) $x=0.03$, (c) $x=0.12$, and (f) $x=0.20$, from Rietveld refinement of NPD data. Note in (c) and (f) the elongation of the monoclinic unit cell along the $(10\bar{1})$ direction of e_g electron polarization at T_N(C-AFM), and in (f) the elongation in the remaining orthorhombic phase of (100) and (001) due to the formation of a (twinned) Wigner-crystal type phase, in contrast to the isotropic monotonic contraction of the G-AFM orthorhombic cell in (a). (d) and (g) T dependence of the phase fraction of symmetry-lowered monoclinic ($P2_1/m$) phase associated with the C-AFM magnetic phase, from the same Rietveld-refinement of NPD data. (b), (e), and (h) T dependence of the integrated intensities of the characteristic G-AFM (110)/(011) (open circles) and C-AFM $(\frac{1}{2}1\frac{1}{2})$ (filled circles) magnetic peaks from NPD data, normalized to the intensity of the strong nuclear (220)/(022) peak, for (b) $x=0.03$, (e) $x=0.12$, and (h) $x=0.20$.

III. RESULTS AND ANALYSIS

A. dc magnetization and resistivity

The T dependencies of the dc magnetization of all studied samples for $H=2000$ Oe are shown in Fig. 2. For $x=0.20$, a peak is observed at $T\sim 180$ K. A similar feature observed for a $Ca_{0.82}Bi_{0.18}MnO_3$ single crystal[24] was ascribed to a change of character of the spin fluctuations from FM to AFM with decreasing T, due to the freezing of the charge carriers and the consequent suppression of DE interactions. At lower T, a sudden enhancement in the dc magnetization is observed below $T_C\sim 110-125$ K for $x\leqslant 0.12$, and is ascribed to a spin-ordering transition with a FM component below T_C. The inset to Fig. 2 shows a dc magnetization at 5 K as a function of H for $x=0.00$, 0.03, and 0.06, with clear signatures of FM components (hysteresis). The x dependence of the dc magnetization at 5 K for $H=2000$ Oe is shown in Fig. 3; results for the large samples used in this study (open markers) are consistent with those for smaller samples previously studied (closed markers).[25]

B. Neutron powder diffraction

At 300 K, the crystal structures of samples at $x=0.00$, 0.03, 0.06, 0.09, 0.12, 0.16, and 0.20 were Rietveld refined as single orthorhombic Pnma phases with TOF NPD data. In preliminary refinements, the O fractional occupancies $[\nu(\mathrm{O})]$ were refined and found to lie between 0.98 and 1.02 for all samples, with typical standard deviations ± 0.008. This result supports the absence of significant cation or oxygen vacancies, consistent with chemical analysis performed on similarly prepared samples,[25] and ν(O) was subsequently fixed at 1.

Figures 4(d) and 4(g) show the crystallographic phase fraction of the symmetry-lowered ($P2_1/m$) phase associated with the C-AFM state, transformed from the orthorhombic Pnma state, for $x=0.12$ and 0.20. This phase transition arises due to the polarization of $d_{3z^2-y^2}$ orbitals along the $(10\bar{1})$ direction, facilitating DE along the FM chains characteristic of C-AFM. A monoclinic phase fraction with a similar T dependence could also be refined for $x=0.09$ and 0.16.

(For $x=0.06$, although the presence of a weak C-AFM magnetic Bragg peak indicates the presence of a small monoclinic phase fraction, this fraction was too small to meaningfully refine.) The transition from the room-temperature orthorhombic P*nma* phase in the C-AFM regime is also shown in the plots of refined lattice parameters vs T in Figs. 4(c) and 4(f). Note that for $x=0.20$ [Fig. 4(f)], in addition to the monoclinic distortion undergone by the majority of the sample, the remaining orthorhombic phase fraction undergoes a different low-T distortion, characterized by an elongation along (100) and (001). This type of distortion has been observed for $Ca_{2/3}La_{1/3}MnO_3$ (Refs. 26 and 27) and $Ca_{1-x}Bi_xMnO_3$ ($x=0.22$ and 0.25) (Ref. 4) at low T, and has been ascribed to superstructures in the *ac* plane caused by charge and orbital ordering of the Mn^{3+} e_g electrons (a ''Wigner crystal''-type or WC-type phase). In order to account for the enlarged unit cell of WC-type without excessively complicating the refinement, the O11 site was split evenly across the $4f$ position. [Although the distortion clearly identifies this phase, no corresponding superstructure Bragg peaks were identified for our $x=0.20$ sample below the orbital-ordering temperature of the WC phase T_O(WC) $\sim$165 K, possibly due to the small phase fraction and/or disorder.]

Final refined crystallographic phase fractions, unit cells, atomic positions, displacement parameters, Mn-O bond distances, and magnetic moments at 20 K for $x=0.03$, 0.12, and 0.20 are given in Table I. The differences between the Mn-O bond distances are very small for the orthorhombic G-AFM phase at $x=0.03$ and 0.12, i.e., the MnO_6 octahedra are not significantly distorted. The same was true of the orthorhombic phases at $x=0.06$ and 0.09 at 20 K (not shown). Conversely, for the monoclinic C-AFM phase at $x=0.20$ and 0.12, as well the monoclinic phases at $x=0.16$, 0.09, and 0.06 (not shown), the Mn1-O12 and Mn2-O12 bonds are longer than the other Mn-O bond distances by $\sim$0.01–0.05 Å, i.e., the MnO_6 octahedra are elongated along the $(10\bar{1})$ direction. This follows from the co-operative Jahn-Teller ordering along $(10\bar{1})$ that allows FM DE in the C-AFM state, and is consistent with previous diffraction studies for electron-doped $CaMnO_3$.[5,28] Finally, for the orthorhombic WC-type phase at $x=0.20$, bond distances from Mn1 to the split O11 site illustrate the alternately shortened and elongated bonds along (101) and $(10\bar{1})$ characterizing this structure type and causing the elongation of a and c relative to $b/\sqrt{2}$ [see Fig. 4(f)].

The magnetic phases of the samples were also identified and Rietveld-refined by NPD, magnetic Bragg peaks being observed at low T for all samples. Observed magnetic reflections were consistent with G-AFM for $x=0.00$ and 0.03, and with C-AFM for $x=0.20$ and 0.16. For intermediate dopings $x=0.06$, 0.09, and 0.12, G- and C-AFM Bragg reflections were observed simultaneously at low T (an extremely weak G-AFM peak was also observed for $x=0.16$). Figure 5 shows a portion of the TOF NPD pattern at high d spacing (low Q) at 20 K for $x=0.12$, illustrating the coexistence of Bragg peaks from distinct C- and G-AFM structures (dots); the solid lines in the upper set correspond to calculated and difference profiles using a magnetic model with phase-separated G- and C-AFM structures. Deficiencies in the fit shown in the upper set of Fig. 5 are accounted for when a FM sublattice with spins perpendicular to those of the G-AFM lattice is included in the magnetic model (lower set). Significant FM intensities were also observed for $x=0.06$ and 0.09 (not shown). This is consistent with our DC-magnetization measurements, where the strongest FM signal was observed for x between 0.06 and 0.12 (see Fig. 3). No evidence was found for a FM moment in the monoclinic phase, as expected, all e_g electrons participating in FM DE along the $(10\bar{1})$ chain directions of C-AFM rather than forming FM clusters.

Figures 4(b), 4(e), and 4(h) show the T dependencies of characteristic Bragg reflections associated with G- and C-AFM spin structures for $x=0.03$, 0.12, and 0.20 respectively. The magnetic ordering temperatures for G-AFM, T_N(G), correspond to the FM T_C observed by dc-magnetization measurements (see Fig. 2) within experimental error. In contrast, the C-AFM order parameter for $x=0.12$, besides showing a rather peculiar T dependence, is far more evident in the NPD than in the magnetization data. Note nonetheless that for $x=0.20$, T_N(C)$\sim$180 K obtained by NPD is clearly associated with the peak in the dc magnetization [compare Figs. 4(h) and 2(a)].

IV. DISCUSSION

A. Sample homogeneity

The relationships among crystal lattices, crystallographic phase fractions and magnetic order parameters as functions of T presented in Fig. 4 reveal relationships that bear on the compositional homogeneity of the polycrystalline samples used in this study. In particular, for 0.12 and 0.20 [Figs. 4(d) and 4(g)], the growth of the monoclinic phase fraction does not continue down to the lowest temperatures. For $x=0.12$ the phase fraction does not change significantly below $\sim T_N$(G-AFM), and for $x=0.20$ it does not change significantly below T_O(WC). Furthermore, for $x=0.12$, T_N(G-AFM) (marked by the dashed line) appears to influence both the C-AFM magnetization [Fig. 4(e)] and the monoclinic lattice parameters [Fig. 4(c)]. These relationships imply that the different magnetic states are competing for the same domains within the sample, rather than simply forming in mutually exclusive, compositionally segregated, domains.

The wide x interval over which P*nma* and $P2_1/m$ crystallographic phases coexist, which is typical of doped manganites, e.g., $Ca_{1-x}Bi_xMnO_3$ (Ref. 4) and $Ca_{1-x}Sm_xMnO_3$,[13] cannot be understood in terms of mesoscopic inhomogeneities in composition x within polycrystalline samples; rather, mesoscopic phase separation at low T is an intrinsic feature of electron-doped manganite perovskites, or at least of these systems where electron doping is accomplished by compositional variation (phase separation might be favored by local chemical variations). The very recent study of $Ca_{1-x}Sm_xMnO_3$, $x=0.15$, by Algabarel *et al.*[29] provides similar evidence for the existence of monoclinic C-AFM and orthorhombic FM-canted G-AFM in phase sepa-

TABLE I. Results from Rietveld refinements of TOF NPD data collected at 20 K for $Ca_{1-x}La_xMnO_3$ samples at selected values of x. Refinements were carried out in space groups Pnma (#62) (atomic positions: O11 in $8d$, O21 in $4c$) and P$2_1/m$ (#12) (atomic positions: O11 in $4f$, O12 in $4f$, O21 in $2e$, O22 in $2e$). G-AFM moments refined along (001), FM along (010), and C-AFM along $(10\bar{1})$. Superscript letters indicate constraints.

x	0.03	0.12		0.20	
Phase fraction	1	0.516(14)	0.484(14)	0.807(3)	0.193(3)
Space group	Pnma	Pnma	P$2_1/m$	P$2_1/m$	Pnma
μ (μ_B/Mn)	G-AFM 2.47(3)	G-AFM 2.45(8) +FM 0.9(2)	C-AFM 2.29(7)	C-AFM 2.89(5)	-
a (Å)	5.27940(9)	5.2933(5)	5.3100(6)	5.34495(17)	5.3916(8)
b (Å)	7.44029(12)	7.4731(6)	7.4537(7)	7.4617(2)	7.4585(5)
c (Å)	5.25978(8)	5.2777(3)	5.3218(8)	5.33475(18)	5.3561(2)
β (°)	-	-	90.8457(18)	91.3109(19)	-
LaCa1 x	0.0327(3)	0.0323(14)	0.030(3)	0.019(2)	0.0360(16)
LaCa1 z	0.9956(8)	0.9964(19)	0.989(3)	0.004(2)	0.9877(16)
LaCa2 x	-	-	0.524(3)	0.523(2)	-
LaCa2 z	-	-	0.510(3)	0.509(2)	-
O11 x	0.2860(2)	0.2879(9)	0.2799(17)	0.2799(11)	0.288(12)/ 0.271(5)
O11 y	0.03433(19)	0.0314(5)	0.0378(15)	0.0402(10)	0.022(6)/ 0.042(6)
O11 z	0.7128(3)	0.7116(8)	0.7162(17)	0.7214(12)	0.743(6)/ 0.699(6)
O12 x	-	-	0.7807(18)	0.7839(6)[a]	-
O12 y	-	-	0.0355(12)	0.0294(8)	-
O12 z	-	-	0.7796(17)	0.7839(6)[a]	-
O21 x	0.4899(4)	0.4866(12)	0.495(3)	0.4864(19)	0.494(4)
O21 z	0.0678(5)	0.0678(13)	0.065(2)	0.0639(18)	0.053(4)
O22 x	-	-	0.998(2)	0.9951(18)	-
O22 z	-	-	0.447(2)	0.438(2)	-
Mn B_{iso}	0.20(3)	0.22(7)[d]	0.22(7)[d]	0.20(6)[b]	0.20(6)[b]
LaCa B_{iso}	0.39(2)	0.35(7)[e]	0.35(7)[e]	0.36(6)[c]	0.36(6)[c]
O11 B_{iso}	0.29(9)	0.19(7)[f]	0.19(7)[f]	0.50(8)	0.3(2)
O12 B_{iso}	-	-	0.19(7)[f]	0.29(7)	-
O21/22 B_{iso}	0.45(4)	0.19(7)[f]	0.19(7)[f]	0.31(8)	0.4(2)
Mn1-O11 (Å) $\sim\parallel(101)$	1.8970(13)	1.904(5)	1.888(9)	1.908(6)	2.03(2)/ 1.83(3)
Mn1-O12 (Å) $\sim\parallel(10\bar{1})$	1.9034(13)	1.906(4)	1.921(9)	1.938(3)	-
Mn1-O22 (Å) $\sim\parallel(010)$	1.8947(5)	1.9035(13)	1.885(2)	1.895(2)	1.886(3)
Mn2-O11 (Å) $\sim\parallel(101)$	-	-	1.916(9)	1.898(6)	-
Mn2-O12 (Å) $\sim\parallel(10\bar{1})$	-	-	1.928(9)	1.939(3)	-
Mn2-O21 (Å) $\sim\parallel(010)$	-	-	1.896(2)	1.8980(18)	-
R_B	0.0672	0.0612		0.0833	
wR_B	0.0700	0.0574		0.0843	
χ^2	1.69	1.88		3.16	

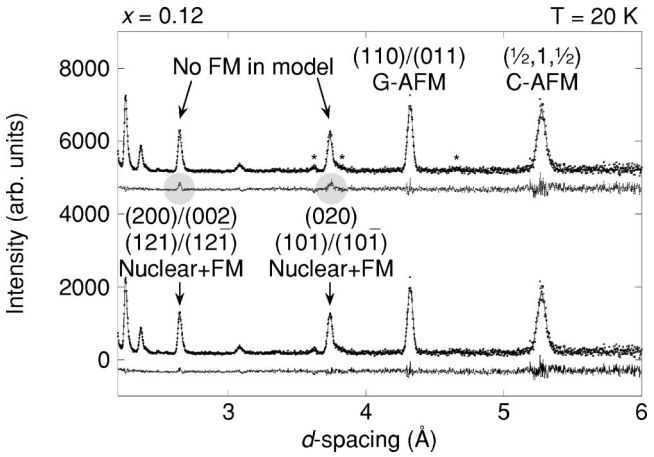

FIG. 5. Observed (+), calculated, and difference (below) plots of Rietveld-refined time-of-flight NPD data (60° detector bank of SEPD) for the $x=0.12$ sample at 20 K. Prominent magnetic reflections are labeled. The upper set shows the fit using a G-AFM + C-AFM magnetic model only, and the bottom set shows the fit with an additional FM component perpendicular to the G-AFM moment. Magnetic reflections due to the AFM Marokite impurity phase are marked (*).

rated regions of compositionally homogeneous samples by demonstrating that their relative phase fractions could be influenced by an external applied magnetic field. There may be some compositional separation at low-x because lighter doping gives a higher probability of La clustering [as recently demonstrated in $La_{1-x}Sr_xMnO_3$ (Ref. 30)], however, the significance of this decreases with increasing x. The competing magnetic states are extremely finely balanced over a broad crossover regime $0.06 \leqslant x \leqslant 0.16$, within which samples do not settle into single thermodynamically stable phases at low T.

B. Spin-lattice coupling and frustration

The competition between orthorhombic G-AFM and monoclinic C-AFM [Fig. 4(d)] reflects the balance of gains and losses associated with the cooperative JT distortion of the latter; a lowering in exchange energy on the one hand, and an increase in elastic energy on the other. This balance is affected by the relative strengths of FM DE and AFM SE interactions. The formation of the monoclinic phase below T_N(C-AFM) corresponds to the ordering of FM DE interactions (which exist as short-range fluctuations above T_N [C-AFM) (Ref. 24)] into infinite one-dimensional (1D) chains, by AFM SE interactions perpendicular to them. The monoclinic phase fraction grows as T decreases because these AFM SE interactions become stronger, decreasing the exchange energy of the monoclinic phase and making its total energy less than that of the paramagnetic orthorhombic phase. At T_N(G-AFM), however, the monoclinic phase fraction of the $x=0.12$ sample stops growing because AFM SE interactions become strong enough to stabilize G-AFM in the remaining orthorhombic phase fraction. This lowers the exchange energy and therefore the total energy of the orthorhombic phase, restoring its status as the more stable crystallographic polymorph. Similarly, in the $x=0.20$ sample [Fig. 4(d)], the monoclinic phase fraction stops growing at T_O(WC) because the distortion required to form the W-C phase is less energetically costly than that required to form C-AFM.

The effects of T_N(G-AFM) on the distortion of the pseudo-cubic lattices, as seen in Figs. 4(a) and 4(c), are also of interest. The G-AFM structure is isotropic and therefore should not effect the lattice, as is indeed the case for $x=0.03$ [Fig. 4(a)]. For $x=0.12$, however, there seems to be a small but significant magnetostrictive effect at T_N(G-AFM) [Fig. 4(c)], whereby the (010) axis elongates slightly relative to (101). This effect may be real, given that (010) is the preferred direction of the net FM moment in the FM cluster glass observed in this composition range (to be discussed in Part II) (Ref. 16); however, since the effect is small, speculation on a mechanism will be avoided. More surprising is the large effect of T_N(G-AFM) on the distortion of the monoclinic lattice [Fig. 4(c)], where no FM clusters are involved. Note, first, that the monoclinic phase does not adopt the fully ordered C-AFM state immediately upon symmetry lowering. This is clear for the $x=0.20$ sample, for which the magnetic order parameter [Fig. 4(h)] and monoclinic distortion [Fig. 4(f)] show strong T dependencies below T_O(WC) [Fig. 4(g)], despite the fact that the monoclinic phase fraction no longer grows. In this light, the refined monoclinic cell for $x=0.12$ [Fig. 4(c)] might actually represent an *average* monoclinic cell, for which a reduction in the monoclinic distortion would not necessarily represent a deterioration of established C-AFM ordered domains. It could simply be a convolution of the delay between symmetry lowering and the establishment of a fully ordered C-AFM state on the one hand, and the increasing strength of the competing G-AFM state on the other hand.

An intriguing extension of this argument is the possibility that the increasing strength of AFM SE interactions as T decreases not only slows the establishment of long-range FM DE (i.e C-AFM) in the monoclinic phase, but actually leads to the establishment of G-AFM there instead. In the extreme case, G-AFM would replace established C-AFM domains. While there is no direct evidence for this in the present data, the reader's attention is brought to the highly analogous ''bilayered'' manganite perovskite $La_{2-2x}Sr_{1+2x}Mn_2O_7$, where the C-AFM phase also requires a symmetry-lowering transition (from tetragonal to orthorhombic).[31] A 10% electron-doped sample in this system ($x=0.90$) exhibited not only a structural transition followed by two magnetic transitions T_N(C-AFM) $=110$ K and T_N(G-AFM) $=60$ K, but a clear *decrease* in the C-AFM order parameter below T_N(G-AFM); i.e., the G-AFM state ''colonizes'' the monoclinic regions established by C-AFM orbital polarization at higher T.

Low-T phase inhomogeneities ultimately arise because short-range FM DE correlations appear at higher T than AFM SE correlations, as has been noted in studies of weak diffuse neutron scattering above the magnetic long-range-ordering transition temperatures.[16,24,29] The C-AFM magnetic state can form at a higher temperature than the G-AFM state because the AFM interactions only have to be strong enough to create AFM order in two-dimensions, rather than

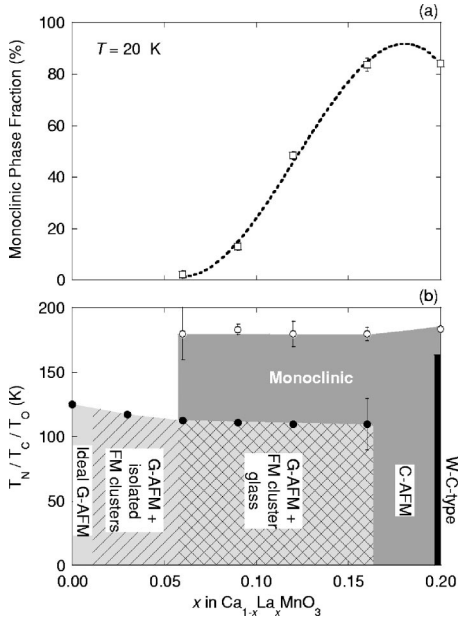

FIG. 6. (a) Refined monoclinic phase fraction at 20 K as a function is x. (b) Ground state phase diagram of $Ca_{1-x}La_xMnO_3$, $0.0 \leqslant x \leqslant 0.2$, mapped onto the crystallographic and magnetic phase transitions determined from NPD data. Closed circles represent the coincident magnetic transitions T_N(G-AFM) and T_C, and open circles represent the coincident magnetic transition T_N(C-AFM) and structural transition T_O. Monoclinic (as opposed to orthorhombic) regions are dark gray. Isolated FM clusters and a FM cluster glass (to be discussed in Part II) (Ref. 16) are indicated by diagonal black lines and black diagonal cross-hatching, respectively. The WC-type phase is black. Note that at the high-x end of the G-AFM regime, the stability of the C-AFM state is very high, and therefore very little G-AFM is actually observed (a); the same is true for the W-C-type at $x=0.20$, and the converse is true at the low-x end of the C-AFM regime.

three-dimensions. At the same time, the strength of the FM SE interactions is obviously related to the concentration of e_g electrons (x) facilitating it. Magnetic and crystallographic ground states are frustrated in the region where 1D FM SE interactions are strong enough to cause e_g orbital polarization and symmetry-lowering at T_N(C), but where AFM DE is strong enough to create 3D order below T_N(G-AFM). This frustration is illustrated by Fig. 6, where the phase diagram [Fig. 6(b)] shows orthorhombic G-AFM to be the ground state for x up to 0.16, but Fig. 6(a) shows that less than 20% of the $x=0.16$ sample is actually in this state at low T. (The incorporation of the FM component observed in electron-doped G-AFM into this phase diagram as isolated FM clusters and a FM cluster-glass is the subject of Part II.)

V. CONCLUSION

Part I of this study used TOF NPD data in conjunction with physical property measurements to identify and characterize the long-range-ordered low-T phases present in samples of $Ca_{1-x}La_xMnO_3$ ($0.00 \leqslant x \leqslant 0.20$). The following Part II presents a neutron-scattering study of short-range features of these phases.[16] The samples appear to be compositionally homogeneous and yet display multiple low-T magnetic states, exemplifying the delicate balance among competing interactions characteristic of the CMR manganites. The results, in conjunction with those of Part II, have been used to construct a ground state phase diagram.

The theme that emerges from this phase diagram is the strong effect that the introduction of FM DE interactions has on the AFM SE (for ideal G-AFM at $x=0$). In orthorhombic G-AFM these FM interactions create 0D correlations; they have no influence on the long-range magnetic structure until the AFM SE interactions become strong enough below T_N(G-AFM) to create long-range 3D AFM order, at which point they are ''frozen in'' as isolated FM clusters, or (in sufficient densities) as an FM cluster-glass (to be discussed in Part II). In monoclinic C-AFM they become 1D in character, leading to $d_{3z^2-r^2}$ orbital polarization and hence symmetry-lowering. At the low-x end of the C-AFM regime, the actual thermodynamic ground state is G-AFM, but this is frustrated by the irreversible structural phase transition favoring C-AFM. In each case, FM DE interactions play a privileged role because they appear at higher T than the competing AFM SE interactions, allowing them to influence the structure on cooling and pre-dispose the system to a particular low-T state.

The changing dimensionality of the FM DE interactions with x, from 0D in the electron-doped G-AFM regime to 1D in the C-AFM regime, foreshadows the subsequent change to 2D [for the A-AFM state at $x \sim \frac{1}{2}$ in some manganite perovskite systems, e.g., $Sr_{1-x}Pr_xMnO_3$ (Ref. 14)] and finally 3D (for the FM state at $\frac{1}{2} < x < 1$ in most such systems). Between the fully-electron-doped (exhibiting a different type of A-AFM) and stoichiometric $CaMnO_3$ (G-AFM) end members, these changes in DE dimensionality with e_g electron concentration underlie the magnetic phase diagram of the CMR manganites. At the same time, the ordering of these e_g electrons via the JT effect underlies the crystallographic phase diagram. The C-AFM, A-AFM, and FM magnetic states are examples of cooperation between these spin and orbital ordering effects, while the phase diagram is also punctuated by regions in which they compete, notably the C-E state at $x \sim 0.5$ and its WC variants between the C-E and C-AFM regimes.

ACKNOWLEDGMENTS

This work was supported by the U.S. Department of Energy, Basic Energy Sciences - Materials Sciences, under Contract No. W-31-109-ENG-38 (CDL, DNA), by the National Science Foundation (NSF) under CAREER Grant DMR 9982834 (JJN) and by CNPq and FAPESP-Brazil (EG). Work at the University of Maryland was supported in part by the NSF MRSEC, DMR 00-80008. The authors thank S. Short of IPNS for technical support in the collection of NPD data.

*Electronic address: ling@ill.fr

[1] P.-G. de Gennes, Phys. Rev. **118**, 141 (1960).
[2] S.-W. Cheong and H.Y. Hwang, in *Colossal Magnetoresistive Oxides*, edited by Y. Tokura (Gordon and Breach, London, 1999).
[3] K. Hagdorn, D. Hohlwein, J. Ihringer, K. Knorr, W. Prandl, H. Ritter, H. Schmid, and T. Zeiske, Eur. Phys. J. B **11**, 243 (1999).
[4] P.N. Santhosh, J. Goldberger, P.M. Woodward, T. Vogt, W.P. Lee, and A.J. Epstein, Phys. Rev. B **62**, 14 928 (2000).
[5] C. Martin, A. Maignan, M. Hervieu, B. Raveau, Z. Jirak, A. Kurbakov, V. Trounov, G. Andre, and F. Bouree, J. Magn. Magn. Mater. **205**, 184 (1999).
[6] M. Respaud, J.M. Broto, H. Rakoto, J. Vanacken, P. Wagner, C. Martin, A. Maignan, and B. Raveau, Phys. Rev. B **63**, 144426 (2001).
[7] C. Martin, A. Maignan, M. Hervieu, B. Raveau, Z. Jirak, M.M. Savosta, A. Kurbakov, V. Trounov, G. Andre, and F. Bouree, Phys. Rev. B **62**, 6442 (2000).
[8] E.O. Wollan and W.C. Koehler, Phys. Rev. **100**, 545 (1955).
[9] J.B. Goodenough, Phys. Rev. **100**, 564 (1955).
[10] A. Maignan, C. Martin, F. Damay, and B. Raveau, Chem. Mater. **10**, 950 (1998).
[11] H. Chiba, M. Kikuchi, K. Kusaba, Y. Muraoka, and Y. Syono, Solid State Commun. **99**, 499 (1996).
[12] H. Aliaga, M.T. Causa, B. Alascio, H. Salva, M. Tovar, D. Vega, G. Polla, G. Leyva, and P. Konig, J. Magn. Magn. Mater. **226**, 791 (2001).
[13] R. Mahendiran, A. Maignan, C. Martin, M. Hervieu, and B. Raveau, Phys. Rev. B **62**, 11 644 (2000).
[14] C. Martin, A. Maignan, M. Hervieu, and B. Raveau, Phys. Rev. B **60**, 12 191 (1999).
[15] D.A. Filippov, R.Z. Levitin, A.N. Vasil'ev, T.N. Voloshok, H. Kageyama, and R. Suryanarayanan, Phys. Rev. B **65**, 100404 (2002).
[16] E. Granado, C.D. Ling, J.J. Neumeier, D.N. Argyriou, J.W. Lynn, and P.L. Lee, following paper, Phys. Rev. B **68**, 134440 (2003).
[17] M. Hennion, F. Moussa, G. Biotteau, J. Rodríguez-Carvajal, L. Pinsard, and A. Revcolevschi, Phys. Rev. Lett. **81**, 1957 (1998).
[18] M. Hennion, F. Moussa, J. Rodríguez-Carvajal, L. Pinsard, and A. Revcolevschi, Phys. Rev. B **56**, R497 (1997).
[19] M. Hennion, F. Moussa, G. Biotteau, J. Rodríguez-Carvajal, L. Pinsard, and A. Revcolevschi, Phys. Rev. B **61**, 9513 (2000).
[20] A. Maignan, C. Martin, F. Damay, B. Raveau, and J. Hejtmanek, Phys. Rev. B **58**, 2758 (1998).
[21] M.-M. Couffon, G. Rocher, and J. Protas, C. R. Hebd. Seances Acad. Sci. **258**, 1847 (1964).
[22] G. Lepicard and J. Protas, Bull. Soc. Fr. Mineral. Cristallogr. **89**, 318 (1966).
[23] C.D. Ling, J.J. Neumeier, and D.N. Argyriou, J. Solid State Chem. **160**, 167 (2001).
[24] W. Bao, J.D. Axe, C.H. Chen, and S.-W. Cheong, Phys. Rev. Lett. **78**, 543 (1997).
[25] J.J. Neumeier and J.L. Cohn, Phys. Rev. B **61**, 14 319 (2000).
[26] P.G. Radaelli, D.E. Cox, L. Capogna, S.-W. Cheong, and M. Marezio, Phys. Rev. B **59**, 14 440 (1999).
[27] M.T. Fernández-Díaz, J.L. Martínez, J.M. Alonso, and E. Herrero, Phys. Rev. B **59**, 1277 (1999).
[28] M. Pissas, G. Kallias, M. Hofmann, and D.M. Tobbens, Phys. Rev. B **65**, 064413 (2002).
[29] P.H. Algarabel *et al.*, Phys. Rev. B **65**, 104437 (2002).
[30] T. Shibata, B. Bunker, J.F. Mitchell, and P. Schiffer, Phys. Rev. Lett. **88**, 207205 (2002).
[31] C.D. Ling, J.E. Millburn, J.F. Mitchell, D.N. Argyriou, J. Linton, and H.N. Bordallo, Phys. Rev. B **62**, 15 096 (2000).